Published in final edited form as:

J Am Chem Soc. 2023 July 12; 145(27): 14932–14944. doi:10.1021/jacs.3c04640.

Acetylation Targeting Chimera Enables Acetylation of the Tumor Suppressor p53

Md Kabir[#],
Mount Sinai Center for Therapeutics Discovery, Department of Pharmacological Sciences, Icahn School of Medicine at Mount Sinai, New York, New York 10029, USA

Ning Sun[#],
Mount Sinai Center for Therapeutics Discovery, Department of Pharmacological Sciences, Icahn School of Medicine at Mount Sinai, New York, New York 10029, USA

Xiaoping Hu[#],
Mount Sinai Center for Therapeutics Discovery, Department of Pharmacological Sciences, Icahn School of Medicine at Mount Sinai, New York, New York 10029, USA

Tiphaine C. Martin,
Department of Oncological Sciences, Tisch Cancer Institute, Icahn School of Medicine at Mount Sinai, New York, New York 10029, USA

Jingjie Yi,
Institute for Cancer Genetics, Department of Pathology and Cell Biology, and Herbert Irving Comprehensive Cancer Center, Vagelos College of Physicians & Surgeons, Columbia University, New York, New York 10032, USA

Yue Zhong,
Department of Oncological Sciences, Tisch Cancer Institute, Icahn School of Medicine at Mount Sinai, New York, New York 10029, USA

Yan Xiong,
Mount Sinai Center for Therapeutics Discovery, Department of Pharmacological Sciences, Icahn School of Medicine at Mount Sinai, New York, New York 10029, USA

H. Ümit Kaniskan,
Mount Sinai Center for Therapeutics Discovery, Department of Pharmacological Sciences, Icahn School of Medicine at Mount Sinai, New York, New York 10029, USA

Corresponding Author Jian Jin — Mount Sinai Center for Therapeutics Discovery, Department of Pharmacological Sciences, Icahn School of Medicine at Mount Sinai, New York, New York 10029, USA; Department of Oncological Sciences, Tisch Cancer Institute, Icahn School of Medicine at Mount Sinai, New York, New York 10029, USA; jian.jin@mssm.edu.

[#]Author Contributions

M.K., N.S., and X.H. contributed equally to this work.

Supporting Information

The Supporting Information is available free of charge at https://pubs.acs.org/doi/10.1021/jacs.3c04640.

Additional experimental details, materials and methods, including Figures S1-S7, Table S1, and ^{1}H NMR, ^{13}C NMR, and LC-MS spectra of MS78 (PDF)

The authors declare the following competing financial interest(s): J.J. is a cofounder and equity shareholder in Cullgen, Inc., a scientific company.

Wei Gu,
Institute for Cancer Genetics, Department of Pathology and Cell Biology, and Herbert Irving Comprehensive Cancer Center, Vagelos College of Physicians & Surgeons, Columbia University, New York, New York 10032, USA

Ramon Parsons,
Department of Oncological Sciences, Tisch Cancer Institute, Icahn School of Medicine at Mount Sinai, New York, New York 10029, USA

Jian Jin
Mount Sinai Center for Therapeutics Discovery, Department of Pharmacological Sciences, Icahn School of Medicine at Mount Sinai, New York, New York 10029, USA; Department of Oncological Sciences, Tisch Cancer Institute, Icahn School of Medicine at Mount Sinai, New York, New York 10029, USA

Abstract

With advances in chemically induced proximity technologies, heterobifunctional modalities such as proteolysis targeting chimeras (PROTACs) have been successfully advanced to clinics for treating cancer. However, pharmacologic activation of tumor-suppressor proteins for cancer treatment remains a major challenge. Here, we present a novel Acetylation Targeting Chimera (AceTAC) strategy to acetylate the p53 tumor suppressor protein. We discovered and characterized the first p53Y220C AceTAC, MS78, which recruits histone acetyltransferase p300/CBP to acetylate the p53Y220C mutant. MS78 effectively acetylated p53Y220C lysine 382 (K382) in a concentration-, time-, and p300-dependent manner and suppressed proliferation and clonogenicity of cancer cells harboring the p53Y220C mutation with little toxicity in cancer cells with wild-tvoe o53. RNA-seq studies revealed novel p53Y220C-dependent upregulation of TRAIL apoptotic genes and downregulation of DNA damage response pathways upon acetylation induced by MS78. Altogether, the AceTAC strategy could provide a generalizable platform for targeting proteins, such as tumor suppressors, via acetylation.

Graphical Abstract

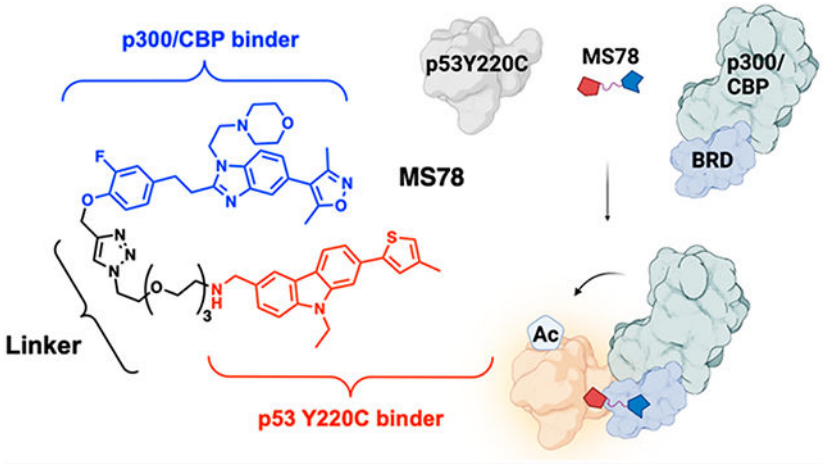

1. INTRODUCTION

Since the concept of targeted protein degradation was proposed,[1] the proteolysis-targeting chimera (PROTAC) field has seen explosive growth over the past 20 years.[2,3] PROTACs are heterobifunctional small molecules that induce a ternary complex between a protein of interest (POI) and an E3 ligase, resulting in polyubiquitination of the POI and its subsequent proteasomal degradation.[2,4] Multiple PROTACs as novel therapeutic modalities for the treatment of cancer have advanced to clinical development.[3] Inspired by the success of PROTACs, several new chemically induced proximity (CIP) technologies have emerged to reprogram the endogenous biological system by inducing protein post-translational modifications (PTMs) in order to potentially treat challenging diseases. Examples of evolving PTM-CIP technologies include deubiquitinase-targeting chimera (DUBTAC),[5,6] phosphorylation-inducing chimeric small molecules (PHICS),[7] protein phosphatase-recruiting chimeras (PHORCs)[8], and a chemo-genetic approach to induce acetylation (AceTAG).[9] However, heterobifunctional small molecules that directly induce acetylation of target proteins in endogenous cellular systems which are not genetically manipulated are unprecedented. The acetylation of historically undruggable tumor suppressor proteins such as p53 could potentially activate these tumor suppressors, leading to a new potential therapeutic strategy for the treatment of cancer.

Lysine acetylation is a dynamic PTM that is generated when an acetyl group from acetyl-CoA is transferred to the ε-amino side chain of lysine by an acetyltransferase, resulting in the regulation of distinct protein properties.[10] Particularly, lysine acetylation functionally regulates important tumor suppressor proteins such as retinoblastoma protein (Rb), phosphatase and tensin homologue deleted on chromosome 10 (PTEN), and p53.[11-13] The tumor suppressor protein p53 plays a critical role as the “guardian of genome” in regulating cell growth, DNA damage, and cell division and commencing appropriate responses to internal and external stimuli.[14] Studies have shown that (1) p53 lysine acetylation in response to DNA damage can effectively bind the p21 promoter region to regulate the cell cycle both *in vitro* and *in vivo*,[15] (2) p53 lysine acetylation can also lead to the destabilization of the p53-MDM2 complex, which regulates p53 protein stability during DNA damage and, thus, induces tumor cell growth arrest and apoptosis,[16] and (3) acetylation of only one of the p53 lysine residues can retain ferroptosis response by regulating *SLC7A11* gene expression.[17] Overall, p53 lysine acetylation is crucial and indispensable for the p53-mediated tumor response and ferroptosis.

Wang et al. previously reported a chemo-genetic approach to induce acetylation (termed AceTAG),[9] based on the published degradation TAG (dTAG) technology.[18] AceTAG utilizes a small-molecule ligand that recognizes the engineered $FKBP12^{F36V}$ variant fused to a POI to study protein acetylation in cells.[9,19] While it is a valuable chemo-genetic tool, AceTAG requires an engineered tagging system via genetic manipulation, making it difficult to be translated into therapeutics.[9] In this study, we introduce a novel small-molecule-based heterobifunctional modality, termed acetylation targeting chimera (AceTAC), which directly induces acetylation of a POI by hijacking an acetyltransferase without the need of any genetic manipulation. We applied this technology to target the p53 Y220C mutant. Y220C, a p53 DNA binding domain (DBD) mutation, is one of the most common

p53 hotspot mutations, which results in the loss of p53 DNA-binding affinity due to thermal instability and affects approximately 125,000 cancer patients annually.[20] While significant progress has been made in developing p53Y220C small-molecule stabilizers,[21-27] p53Y220C AceTAC represents a different type of therapeutic modalities, which could have more profound antitumor activities compared to p53Y220C small-molecules stabilizers by acetylating p53Y220C. Our lead compound, MS78, which simultaneously binds p53Y220C and the bromodomain of histone acetyltransferases CREB (cyclic-AMP response element binding protein) binding protein (CBP)/E1A binding protein (p300) (CBP/p300), effectively acetylated p53Y220C in a concentration- and time-dependent manner. MS78 induced cell growth arrest in a p53- and p300-dependent manner and was more potent than the parent p53 stabilizer in suppressing the growth and clonogenicity of pancreatic and gastric cancer cells. Using RNA-seq studies, we found that the acetylation induced by MS78 led to p53Y220C-depedent upregulation of TRAIL apoptosis genes and heat shock protein processing in the endoplasmic reticulum while simultaneously downregulating the DNA damage response repair (DDR) pathway. Overall, MS78 as the first p53Y220C AceTAC is a valuable chemical tool to study the functions of p53Y220C acetylation and could be further developed into a potential treatment for cancers harboring the Y220C mutation. AceTAC is a novel approach and could provide a generalizable platform to target tumor suppressor proteins via acetylation.

2. RESULTS AND DISCUSSION

2.1. Rational Design of p53Y220C-Targeting AceTACs.

The mutation of tyrosine to cysteine at residue 220 results in a druggable cavity on the surface of p53, and it was previously shown that a carbazole-based scaffold can bind the cavity and restore the thermal stability of p53Y220C to wild-type (WT).[25,28] It was shown that the 7 position of the carbazole scaffold can be occupied with different heterocyclic rings, leading to better binding affinity.[25] Thus, we chose PK9323, which contains a 2-thiazole substituent, as the starting p53Y220C binding ligand because (1) it stabilizes p53Y220C with a melting temperature (T_m) of 3.1 °C, (2) it interacts with the D228 backbone of the p53 DNA binding domain (DBD) (PDB ID: 6SI0), (3) it is a noncovalent, reversible small-molecule binder of p53Y220C, which allows AceTACs to be catalytic, and (4) it is synthetically feasible.[25] Based on the p53Y220C-PK9323 cocrystal structure, we found the methylamine of PK9323 was solvent-exposed and could be utilized to attach a linker (Figure 1A). We chose to hijack histone acetyltransferases p300/CBP to induce p53Y220C acetylation mainly because p300/CBP are highly expressed and are active acetyltransferases for a broad range of substrates.[29-31] To hijack p300/CBP for inducing acetylation, we chose to utilize selective small-molecule binders of the p300/CBP bromodomain, not small-molecule inhibitors of p300/CBP, because p300/CBP bromodomain binders do not inhibit the acetyltransferase activity of p300/CBP, the very activity we aim to harness.[32-34] We analyzed the cocrystal structure of the CBP bromodomain in complex with a small-molecule binder (compound **17**) (PDB ID: 4NR5) (Figure 1B).[35] While the isoxazole moiety of compound **17** forms a key hydrogen bond with the CBP bromodomain, the right-hand side phenyl ring of compound **17** is solvent-exposed. Because compound **33**, which contains the *para*-methoxy- and *meta*-fluoro-substituted

phenyl ring, has higher affinity than compound **17** and was successfully utilized by us to recruit CBP/p300 previously,[36] we chose to use compound **33** instead of compound **17** for AceTAC development. We therefore conjugated different polyethylene glycol (PEG) linkers via an amide bond to the terminal methylamine of PK9323, which were then linked with the methoxy group of compound **33** via a click reaction, to afford compounds **1–4** (Figure 1C, Scheme S1).

To test these compounds, we generated an NCI-H1299 cell line stably expressing the FLAG tagged p53Y220C mutant NCI-H1299 (p53Y220C). The background NCI-H1299 cell line is a p53 null cell line. We observed that compound **3** (PEG-3) and compound **4** (PEG-4) modestly increased p21 expression at 5 μM in the NCI-H1299 (p53Y220C) cell line at 24 h while PK9323 and compounds **1** and **2** did not (Figure 1D). The lack of significant effects could be due to the fact that the extra methyl group on the terminal amine and the amide functionality in compounds **1–4** might impact binding of these compounds to p53Y220C, based on the previously reported structure-activity relationship (SAR) results for the PK9323 series.[25,26] Therefore, we designed a second set of AceTACs, compounds **5–9**, by removing the extra methyl group and amide functionality (Figure 1E, Scheme S2). We were pleased to find that compounds **5–9** increased the expression of p21 by about 2-fold compared to PK9323 at the same concentration (Figure 1F,G). Particularly, compound **7** (PEG-3) at 5 μM induced the most significant acetylation of p53Y220C lysine 382 (p53K382ac) among these compounds (with PK9323 as a control) at 8 h treatment (Figure 1H). Through these initial studies, we demonstrated that our AceTACs can acetylate p53Y220C and induce p21 expression more effectively than parent p53Y220C binder PK9323.

2.2. Discovery of MS78.

After identifying several hits, we sought to discover a more potent and efficacious p53Y220C AceTAC. It was previously reported that the 4-methyl thiophen-2-yl group (in PK9328) led to a higher binding affinity (K_D = 1.7 vs 5.3 μM) and slightly better stabilization of p53Y220C than the thiazo-4-yl group (in PK9323).[25,26] Thus, we replaced the thiazole group of compound **7** with the 4-methyl thiophen-2-yl group, resulting in MS78 (Figure 2A). We were pleased to find that MS78 was indeed more effective in inducing p53Y220C K382 acetylation in the NCI-H1299 (p53Y220C) cell line (Figures 2B and S1). Particularly, MS78, at 10 μM, induced p53K382ac by about 2-fold more compared to compound **7** at 24 h (Figure 2B). Because MS78 is more effective than compound **7** in inducing p53K382ac, we chose to characterize MS78 further as a p53Y220C AceTAC and use it for further biological studies.

To confirm that MS78 binds and stabilizes the p53Y220C protein, we performed a cellular thermal shift assay (CETSA) in the NCI-H1299 (p53Y220C) cell line. Similar to previous results, DMSO-treated p53Y220C had an aggregation temperature (T_{agg}) of 39 °C ± 2 °C (Figure S2).[27] On the other side, both PK9328 and MS78 increased the T_{agg} shift by 4 °C, suggesting that MS78 maintains a similar binding affinity to p53Y22C and a comparable stabilization of p53Y220C compared to that of PK9328 (Figures 2C and S2). Furthermore, MS78 binds the bromodomain (BRD) of CBP/p300 with an IC_{50} of 3.02 ± 0.02 μM in an AlphaScreen binding assay and is selective for the CBP/p300 BRD over a panel of

other BRD-containing proteins (Figure S3). Next, we determined that MS78 induced the p53K382ac level in the NCI-H1299 p53Y220C stable cell line in a concentration-dependent manner with an ACE_{50} (the concentration at which 50% of p53Y220C is acetylated) of 1.87 ± 0.3 μM with the acetylation level induced by MS78 at 10 μM as the maximum response (Figure 2C). In addition, MS78 induced p53K382 acetylation in a time-dependent manner (Figure 2D). MS78 increased the p53K382ac level by about 2-fold as early as 6 h and by about 4-fold within 24 h (Figure 2D). We also conducted a washout experiment by treating NCI-H1299 (p53Y220C) cells with 10 μM MS78 for 6 h, then removing MS78 and monitoring the p53K382ac level over time. We found that the p53K382ac level returned to the baseline DMSO level at 8 h post the MS78 removal (Figures 2E and S4), suggesting that the p53Y220C K382 acetylation induced by MS78 is reversible. It was previously reported that both HDAC6 and SIRT2 can regulate the p53K382ac level.[37,38] Therefore, it would be interesting to further investigate the contribution of deacetylases such as HDAC6 and SIRT2 in regulating the p53 acetylation level after MS78 treatment. Overall, these results demonstrated that MS78 binds p53Y220C and the CBP/p300 bromodomain selectively and effectively induces p53Y220C K382 acetylation in a concentration- and time-dependent manner.

Next, we performed endogenous IP experiments to pull down FLAG-tagged p53Y220C to assess the formation of the ternary complex between p53Y220C and p300 in the presence of MS78. We treated NCI-H1299 p53-null and NCI-H1299 p53Y220C cells with MS78 at two concentrations. As expected, MS78 induced an interaction between p53Y220C and p300 and induced p53K382ac in a concentration-dependent manner in NCI-H1299 p53Y220C cells, whereas no interaction was observed in NCI-H1299 p53-null cells (Figure 2F). To further confirm that p53Y220C K382 acetylation depends on p300, we knocked down p300 using siRNA in the NCI-H1299 (p53Y220C) cell line and monitored p53Y220C K382 acetylation. Upon treatment with MS78, there was a concentration-dependent increase in the p53K382ac level in control siRNA-treated cells concurrent with the increase in interaction between p53Y220C and p300 (Figure 2G). On the other hand, p53Y220C K382 acetylation was significantly diminished in the p300 siRNA-treated cells (Figure 2G), thereby confirming that the MS78-mediated p53Y200C K382 acetylation is dependent on p300. Finally, we performed competition rescue experiments by pretreating the NCI-H1299 p53Y220C cell line with 10 μM compound **33** (the p300/CBP bromodomain binder used in MS78) for 2 h. Compound **33** pretreatment completely abolished the p300-p53Y220C interaction and significantly reduced the p53K382ac level induced by MS78 (Figure 2H). Altogether, the FLAG-IP, knockdown and rescue experiments in the isogenic cell lines demonstrated that MS78 can induce ternary complex formation between p53Y220C and p300, and the p53Y200C K382 acetylation induced by MS78 is dependent on p300. It is worth noting that the exact role of CBP is not clear, and further investigation is needed in the future.

2.3. Antiproliferative Activity of MS78 in p53Y220C-Harboring Cancer Cell Lines.

As MS78 effectively induces p53Y220C K382 acetylation in a p300-dependent manner, we hypothesized that the antiproliferative activity of MS78 also depends on the presence of p53Y220C and p300. Therefore, we assessed the effect of MS78 on the cell viability and p53K382ac level in p53-null and p53Y220C-expressing NCI-H1299 isogenic cell lines

with PK9328 and compound **33** as controls (Figure 3A,B). As expected, in NCI-H1299 p53-null cells, MS78 as well as PK9328 and compound **33** did not induce any significant cell growth inhibition (Figure 3A). On the other hand, in NCI-H1299 p53Y220C cells, MS78 concentration-dependently inhibited the cell growth and was more effective than the parent p53Y220C stabilizer PK9328 in inhibiting the cell growth, while compound **33** had no effect (Figure 3B). We next confirmed that while MS78 did not induce K382 acetylation in NCI-H1299 p53-null cells, it significantly induced K382 acetylation in NCI-H1299 p53Y220C cells (Figure 3C). As expected, PK9328 and compound **33** did not significantly induce K382 acetylation in either cell line (Figure 3C). Furthermore, in p53Y220C-expressing NCI-H1299 cells, knockdown ofp300 abolished the antiproliferative effect of MS78 (Figure 3D,E). Interestingly, PK9328 induced about 50% reduction in the cell growth in p300-siRNA-treated NCI-H1299 p53Y220C cells, confirming that the main mechanism of action of PK9328 is independent of p300 (Figure 3D,E). We also confirmed that the effect of MS78 on inducing p53 Y220C K382 acetylation was abolished in p300 knockdown cells (Figure 3F). Overall, these results suggest that the cell growth inhibition effect of MS78 is dependent on p53Y220C and p300.

Next, we examined the tumor-suppressive effect ofMS78 on p53Y220C-harboring cancer cell lines. Indeed, MS78 exhibited potent antiproliferative activity in BxPC3 (p53Y220C/−) cells with a GI_{50} of 3.3 ± 1 μM and in NUGC-3 (p53Y220C/+) cells with a GI_{50} of 2.7 ± 0.5 μM (Figure 4A-F). Importantly, MS78 displayed about 4-fold higher potency compared to the parent compound PK9328 (GI_{50} of 13.9 ± 2.4 μM in BxPC3; GI_{50} of 12.6 ± 1.9 μM in NUGC-3 cell line), while compound **33** had minimal antiproliferative activity (Figure 4A,D). Consistent with the cell viability results, MS78 also showed a marked reduction in clonogenicity in both BxPC3 and NUGC-3 cell lines compared to PK9328 and compound **33** (Figure 4B,E). The superior antiproliferative effect of MS78 is likely due to its ability to acetylate p53Y220C K382. Indeed, MS78 induced an about 4-fold increase in the p53K382ac level at 10 μM in both BxPC3 and NUGC-3 cell lines (Figure 4C,F).

We next assessed the toxicity of MS78 in cancer cells with wild type (WT) p53 with PK9328 and compound **33** as controls. In p53 WT U-2OS cancer cells, both MS78 and PK9328 did not significantly inhibited cell growth (GI_{50} > 10 μM) with modest inhibition (30–40%) at the highest concentration tested (10 μM) (Figure 4G). As expected, these compounds did not alter the p53K382ac level (Figure 4H). Furthermore, because some p53Y220C small-molecule stabilizers were reported to induce cell death in WI38, a normal fibroblast cell line,[21,22,24] we assessed the cytotoxicity of MS78 in a normal prostate cell line, PNT2. We found that MS78 as well as PK9328 and compound **33** are not toxic in PNT2 cells (GI_{50} > 10 μM) (Figure S5). Taken together, these results suggest that MS78's antiproliferative activity is selective for cancer cells with the Y220C mutation over cancer cells with WT p53 and normal cells and that MS78 could be a potentially useful tool compound for selectively targeting cancer cells harboring the p53Y220C mutation.

2.4. MS78-Induced p53Y220C Acetylation Regulates Unique Signaling Pathways.

It was previously reported that several p53Y220C small-molecule stabilizers could restore the activity of the p53Y220C mutant to WT activity and induce the expression of

PUMA, p21, MDM2, NOXA, and BAX.[23,24,27] To compare the effect of p53Y220C K382 acetylation to traditional p53Y220C stabilization on downstream signaling, we performed RT-qPCR to assess changes in the mRNA levels of p53-target genes upon MS78 and PK9328 treatment. Similar to the previously reported results, we found that the p53Y220C stabilizer PK9328 upregulated the expression of p21 (*CDKN1A*) and *Mdm2* genes (Figure S6). On the other hand, MS78 induced less upregulation in *CDKN1A* and *Mdm2* compared to PK9328, while both MS78 and PK9328 had little or modest effect on *TIGAR, BAX,* and PUMA (*BBC3*) genes (Figure S6). To better understand the global impact of p53Y220C acetylation induced by MS78 on downstream signaling, we performed RNA-seq studies in NCI-H1299 p53-null and p52Y220C-expressing isogenic cell lines treated with MS78.

Using the RNA-seq data, we evaluated and identified enrichment in the 343 high confidence p53-target genes previously reported (q-value < 0.01, normalized enrichment score (NES) = 1.52, Figures 5A-D and S7).[39] We first determined the effect of MS78 on genes regulating the cell cycle process. Similar to the RT-qPCR results, the RNA-seq studies also confirmed the upregulation of the p21 gene (*CDKN1A*) after 10 μM MS78 treatment for 24 h (Figure 5A-C). Furthermore, MS78 treatment also led to the upregulation of several cell-cycle arrest genes such as *GADD45A* and *BTG1* which were previously shown to induce G2/M and G1/S cell cycle arrest.[40,41] Finally, we also determined the p53-dependent repression of *E2F1, CDC25A, CDK1,* and *CDK4* genes indicative of the activation of the p53-p21-DREAM-E2F/CHR (p53-DREAM) repressor pathway.[39,42] However, the p53Y220C stabilizer PK9328 induced a 12-fold increase in p21 mRNA expression, while MS78 induced an 8-fold increase in p21 mRNA expression (Figure S6), suggesting MS78 may lead to other p53Y220C-mediated transcriptomic changes.

Next, we assessed the effect of MS78 on genes regulating apoptosis and found that there was no significant upregulation of BAX, PUMA (*BBC3*), and NOXA (*PMAIP1*) genes, consistent with the RT-qPCR results (Figure S6). However, interestingly, MS78 induced a statistically significant induction of TNF-related apoptosis inducing ligand (TRAIL) genes such as TRAIL-R1 (*TNFRSF10A*), TRAIL-R2 (*TNFRSF10B*), and TRAIL-R4 (*TNFRSF10D*) ($\log_2$ fold change > 2, p-value < 0.05) (Figure 5A,B). It was previously shown that p53 WT has two DNA binding sites on *TNFSF10* promoter regions and can regulate TRAIL gene transcription to induce cell death.[43] Furthermore, it was also demonstrated that acetylation of the gain-of-function (GOF) p53 mutant R158G significantly reduced tumor growth *in vivo* by upregulating TRAIP expression which subsequently suppresses the oncogenic nuclear factor kappa-B (NF-κB) signaling.[44] Our results suggest that p53Y220C K382 acetylation may also prompt cell death by inducing the expression of TRAIL genes.

To our surprise, while MS78 led to the downregulation of several DDR genes, such as *ATM, ATR,* and *CHEK1*/2, we also found the upregulation of several heat shock protein genes, such as *HSPA5,* HSP40 (*DNAJB1*), and *HSP1A1/B* (Figure 5B). Together with the upregulation of heme oxygenase 1 (*HMOX1*) and nuclear protein 1, transcriptional regulator (*NUPR1*) genes upon MS78 treatment, these data suggest that MS78 may regulate ferroptosis response by upregulating key genes such as *HSPA5, HMOX1,* and *NUPR1*.[40,45,46] Further unbiased analysis using differential gene expression (DGE) and

enrichment in KEGG pathways revealed downregulation of the proteins involved in homologous recombination, base excision repair, and DNA replication pathway with simultaneous upregulation of protein processing in the endoplasmic reticulum (ER) compared to DMSO (Figure 5E). To determine the p53Y220C-specific effect of MS78, we compared the MS78-mediated DGE in NCI-H1299 p53Y220C cells relative to that in NCI-H1299 p53-null cells and the DMSO control in both cell lines (Figure 5F). Consistently, MS78 upregulated TRAIL and key ferroptosis genes while downregulating the DDR pathway only in the NCI-H1299 p53Y220C cell line, suggesting that these differentially altered pathways are likely due to the p53Y220C acetylation induced by MS78 (Figure 5F). However, further investigations are needed to validate the downstream targets of p53Y220C K382 acetylation induced by MS78.

3. CONCLUSIONS

In this study, we present the development of AceTAC, a small-molecule-based heterobifunctional modality that directly induces acetylation of a POI by hijacking an acetyltransferase without the need of any genetic manipulation. We applied this technology to target the Y220C mutant of the tumor suppressor p53, one of the most common p53 hotspot mutations, which affects approximately 125,000 cancer patients annually. We discovered and characterized the first p53Y220C AceTAC, MS78, which can effectively acetylate p53 by inducing ternary complex formation between p53Y220C and the acetyltransferases p300/CBP. MS78 induced concentration- and time-dependent p53Y220C K382 acetylation. We show that the p53Y220C K382 acetylation induced by MS78 is dependent on p53Y220C and p300 and is reversible. Our p53Y220C AceTAC MS78 displayed superior antiproliferative effect and suppression of clonogenicity to the parent p53Y220C stabilizer PK9328 in several p53Y220C-harboring cancer cell lines. The cancer cell growth inhibition effect induced by MS78 is dependent on the p53Y220C and p300. MS78 was also not toxic in cancer cells with WT p53 and normal cells. We conducted RNA-seq studies, which revealed that the p53Y220C AceTAC has a novel mechanism of action, induction of TRAIL and ferroptosis genes, and simultaneous downregulation of DDR pathways. While there are numerous studies on understanding WT p53 acetylation, this is the first study that examines the effect of lysine acetylation on the functions of a p53 mutant using a chemical tool. In particular, by conducting the RNA-seq studies in two isogenic cell lines, we show that MS78 led to distinctive transcriptomic changes in the apoptosis, ferroptosis, and DDR pathways. However, further studies are needed to fully characterize the effect of MS78 on regulating gene expression in p53Y220C-harboring cancer cells. It is also worth noting that it is unclear currently whether MS78 induces p53Y220C acetylation at other lysine residues besides K382, and this warrants further investigation. Overall, we successfully applied the novel AceTAC strategy to target p53Y220C and discovered the first p53Y220C AceTAC, MS78, which is a valuable tool compound to further investigate the functions of p53Y220C acetylation in cancers harboring the p53Y220C mutation. Our results suggest that AceTAC could provide a potentially generalizable platform to target tumor suppressor proteins via acetylation. Furthermore, AceTAC could further expand the heterobifunctional small-molecule-induced post-translational modification field.

4. EXPERIMENTAL METHODS

4.1. Compound Synthesis.

Synthesis and characterization of compounds **1–9** and MS78, as well as their intermediates, are detailed in the Supporting Information.

4.2. Cell Lines, Tissue Culture, and Transfection.

NCI-H1299 (CRL-5803), BxPC3 (CRL-1687), and U-2OS (HTB-96) cells were purchased from the American Tissue Culture Collection (ATCC, Manassas, VA). In addition, NUGC-3 cells were obtained from the Japan Health Science Research Resources Bank (JCRB, JCRB0822). NCI-H1299, BxPC3, and NUGC-3 cells were cultured in RPMI 1640 medium (Thermo Fisher Scientific Inc., Waltham, MA) supplemented with 10% Gibco heat-inactivated fetal bovine serum (FBS) (Life Technologies, Grand Island, NY) and 1% Gibco penicillin/streptomycin (Life Technologies, Grand Island, NY). U-2OS cells were cultured in McCoy's 5A (modified) medium (Thermo Fisher Scientific Inc., Waltham, MA) supplemented with 10% heat-inactivated FBS and 1% penicillin/streptomycin. All cells were incubated at 37 °C in a standard humidified incubator containing 5% CO_2 and 95% O_2.

For siRNA transfection, control and p300 siRNA (sc-29431) were purchased from Santa Cruz Biotechnology. Briefly, NCI-H1299 cells were seeded on 6-well plates at a density of 3×10^5 cells/well (~75–80% confluency). Cells were transfected the following day with Lipofectamine 3000 transfection reagent (L3000008, ThermoFisher Scientific) and harvested 48 h after transfection. For the construction of FLAG-p53Y220C stable cell lines, transfected NCI-H1299 cells were selected with G418 for 14 days.

4.3. Antibodies and Immunoblotting.

Total cell lysate was used for Western blots, as previously described.[47] The following primary antibodies were used in the study: Vinculin (Cell Signaling Technology [CST], 13901), p53 (CST, 2527), acetyl-p53 (lys-382) (CST, 2525), acetyl-p53 (lys-379) (CST, 2570), p21 (CST, 2947), p300 (CST, 86377), and p53 polyclonal antibody (Proteintech, 10442-1-AP). Blots were imaged using fluorescence-labeled secondary antibodies on LI-COR Odyssey CLx imaging systems.

4.4. CBP/p300 Binding Assays and Selectivity against Other Bromodomain-Containing Proteins.

CBP/p300 bromodomain binding affinities were determined using the AlphaScreen assay (conducted by Reaction Biology Corp.) as described previously.[35] MS78 was prepared as 10 mM stock in 100% DMSO. K_d values were determined by testing MS78 in duplicates against the bromodomain of CBP/p300 in 10-concentration with a 2-fold serial dilution starting at a concentration of 20 μM. MS78 was further in BromoMelt profiling assay by Reaction Biology Corp. tested against other bromodomain-containing proteins at 10 μM in duplicates.

4.5. CETSA.

The CETSA assays were performed as previously described.[27] Briefly, p53Y220C stable cells were treated with DMSO, PK9328, or MS78 for 1 h, harvested by scraping in PBS, and pelleted. Cells were resuspended in 500 μL of PBS with 1× cOmplete EDTA-free protease inhibitor cocktail (Sigma, #11836170001) and split into 50 μL aliquots in an 8-tube strip (USA Scientific, #1402-4700). The cell suspension was heated with a gradient from 30 to 50 °C in a thermocycler for 3 min and then cooled to 25 °C for 3 min. The heat-treated samples were flash-frozen in liquid nitrogen, thawed at 25 °C, and briefly vortexed. The freeze–thaw cycle was repeated three times in total. Samples were cleared of aggregate by centrifugation at 20,000×g and 4 °C for 20 min. Cleared supernatant (30 μL) was mixed with 5× SDS-loading buffer for WB analysis.

4.6. FLAG Immunoprecipitation.

Endogenous co-IP experiments were performed as described previously.[48] Briefly, 2×10^6 cells were seeded in a 10 cm dish and treated with 0, 1, or 10 μM MS78 for 24 h. Cells were then washed with ice-cold PBS twice and centrifuged at 200×g for 3 min to get cell pellets which were then lysed with 300 μL of lysis buffer (20 mM HEPES, pH 7.4, 150 mM NaCl, 2 mM EDTA, 1% Triton X-100, and EDTA-free phosphotase and protease inhibitor) for 30 min on ice, and centrifuged at 14,000×g for 10 min to get supernatant as cell lysate. The ANTI-FLAG M2 affinity gel (Product #A2220, Sigma-Aldrich, Inc.) was used for the purification of FLAG-p53Y220C, according to the manufacturer's guidelines. Following incubation of M2 affinity gel, protein was eluted using 3× FLAG Peptide (Product #F4799, Sigma-Aldrich, Inc.), and supernatant was resuspended in 30 μL of 1× SDS-PAGE Laemmli buffer for boiling. The protein samples were then tested by WB.

4.7. Cell Viability Assay.

The cell viability assay was performed as previously described.[48] Briefly, 5×10^4 cells were seeded per well into 96-well microplates. After 24 h, cells were treated with 3-fold serially diluted compounds in triplicate for 72 h. Cell viability was evaluated using the WST-8 reagent (CK04, Dojindo). Absorbance signals were obtained with Infinite F PLEX plate reader (TECAN, Morrisville, NC) at 450 nm with 690 nm as reference wavelength after 3 h incubation at 37 °C. GraphPad Prism 8 was used in the analysis of GI_{50} values from the data of three independent experiments.

4.8. Clonogenic Assay.

The clonogenic assay was performed as previously described.[48] BxPC3 or NUGC-3 cells (2000 cells per well) were seeded into 12-well tissue culture plates. After 24 h, cells were treated with 0, 1, 3, and 10 μM of indicated compounds for 14 d. Cell medium was exchanged with fresh full medium containing indicated compounds every 72 h. The plates were then washed with PBS and stained with a solution containing 0.5% (w/v) crystal violet and 6% (v/v) glutaraldehyde for 30 min. The plates were then washed with running water until cell colonies were clear without background color and then dried at room temperature. Epson Perfection V600 Photo was used for the acquisition of the images.

4.9. Quantitative Reverse Transcriptase Polymerase Chain Reaction (RT-qPCR).

The RT-qPCR was performed as previously described.[47,49] Briefly, NCI-H1299 p53Y220C stable cells were treated with DMSO or 10 μM PK9328, compound **17**, or MS78 for 24 h. Total RNA was extracted using the Monarch Total RNA Miniprep Kit (T2010S, New England Biolabs), and cDNA was generated using the SuperScript IV First-Strand Synthesis System (18091050, Thermo Fisher). qPCR was performed using the PowerUp SYBR Green Master Mix (Thermo Fisher Scientific, A25742) on an Agilent Technologies Stratagene Mx3005p qPCR system. RxnReady premixed primer pairs for p53, p21, TIGAR, BAX, PUMA, and MDM2 were purchased from Integrated DNA Technologies, Inc. (Coralville, IA). *GAPDH* forward, 5′-ACAACTTTGGTATCGTGGAAGG-3′, and *GAPDH* reverse, 5′-GCCATCACGCCACAGTTTC-3′, were used as controls. The mRNA expression for each target gene was first normalized to internal GAPDH and then calculated relative to the DMSO control. Experiments were performed in triplicates.

4.10. RNA-seq Study.

NCI-H1299 p53-null and p53Y220C stable cells were treated with DMSO or 10 μM MS78 for 24 h in quadruplicates. Cells were washed three times using ice-cold 1× PBS and subsequently pelleted by centrifuging at 12,000 rpm at 4 °C. The pellet was flash frozen and sent to Azenta Life Sciences for further studies. The total RNA in 16 samples was extracted using a Qiagen RNeasy Plus Mini Kit according to the protocols in the RNeasy Plus Mini Handbook published by Qiagen. RNA-seq libraries were constructed from the PolyA-selected mRNA using the TruSeq RNA sample preparation guide (Illumina), and paired-end 150 base pairs sequencing on a HiSeq2500 system (Illumina) was performed at Azenta Life Sciences. The raw data in FASTQ format was analyzed as previously described.[50]

After quality control of FASTQ files using the FASTQC tool (version 0.11.7) (http://www.bioinformatics.babraham.ac.uk/projects/fastqc/), we trimmed low-quality bases (Phred < 10) and adapter sequences and then discarded short reads (length < 60 nt) using the bbduk tool (version 37.53) (https://jgi.doe.gov/data-and-tools/bbtools/bb-tools-user-guide/). When either the forward or reverse of a paired-end read was discarded, we discarded the complete paired-end read. We quantified the expression of transcripts using cleaned paired-end reads with the Salmon tool (version 0.9.1)[51] using the human reference transcriptome from The Cancer Genome Atlas (TCGA; GDC.h38 GENCODE v22).[52] We performed the differential expression between the NCI-H1299 (p53Y220C) cell lines treated with DMSO or MS78 and the NCI-H1299 (p53-null) cell lines treated with DMSO or MS78 at the gene level using the R tximport library (version 1.26.1) on R (version 4.2.2).[53] We prefiltered genes to keep only genes that had at least 10 reads in total (N_{gene} = 22,454) and then performed differential gene expression using the R DESeq2 library (version 1.38.3). We identified as differential expressed between two conditions when the *P* value adjusted was at 5% and $\log_2$ (fold change) was more than 1. The heatmap was drawn using the R ComplexHeatmap library (version 2.14.0). We next performed GSEA to capture pathways perturbed toward both directions simultaneously using the 22,454 ranked genes identified in our data set and annotated in ENSEMBL (version 94) against the 343 p53 target genes listed in a previously reported study[39] using GSEAPreranked (version 4.3.2.; number of permutations = 1000, no collapse) and the KEGG pathways using R GAGE (version 2.48.0).

4.11. Data Availability.

RNA-seq data have been deposited in the GEO database (GEO accession no. GSE229576). There are no restrictions on the data availability.

4.12. Statistics and Reproducibility.

Experimental data are presented as the mean ± SD or SEM of three independent experiments, unless otherwise noted. Statistical analysis was performed using an unpaired two-sided Student's *t* test for comparing two sets of data with an assumed normal distribution. The results for immunoblotting are representative of at least three biologically independent experiments, unless otherwise noted. All statistical analyses and visualizations were performed using GraphPad (Prism v8.4.2) and BioRender.

Supplementary Material

Refer to Web version on PubMed Central for supplementary material.

ACKNOWLEDGMENTS

This work utilized the NMR spectrometer systems at Mount Sinai acquired with funding from National Institutes of Health SIG Grants 1S10OD025132 and 1S10OD028504. J.J. acknowledges the support by an endowed professorship by the Icahn School of Medicine at Mount Sinai. M.K. acknowledges the support by the National Cancer Institute (NCI)-funded Training Grant in Cancer Biology (T32CA078207). Y.Z. acknowledges the support by the National Institute of General Medical Sciences (NIGMS)-funded Integrated Pharmacological Sciences Training Program T32GM062754. This work was supported in part through the computational and data resources and staff expertise provided by Scientific Computing and Data at the Icahn School of Medicine at Mount Sinai and supported by the Clinical and Translational Science Awards (CTSA) grant UL1TR004419 from the National Center for Advancing Translational Sciences. We would like to acknowledge the help and support of Dr. Jeffrey R. Johnson and Mr. Andrew Kurland at the Icahn School of Medicine at Mount Sinai. We also thank Drs. James J. Manfredi and Yi Shi at the Icahn School of Medicine at Mount Sinai for their helpful advice and suggestions.

REFERENCES

(1). Sakamoto KM; Kim KB; Kumagai A; Mercurio F; Crews CM; Deshaies RJ Protacs: chimeric molecules that target proteins to the Skp1-Cullin-F box complex for ubiquitination and degradation. Proc. Natl. Acad. Sci. U S A 2001, 98 (15), 8554–8559. [PubMed: 11438690]

(2). Dale B; Cheng M; Park KS; Kaniskan H; Xiong Y; Jin J Advancing targeted protein degradation for cancer therapy. Nat. Rev. Cancer 2021, 21 (10), 638–654. [PubMed: 34131295]

(3). Békés M; Langley DR; Crews CM PROTAC targeted protein degraders: the past is prologue. Nat. Rev. Drug. Discovery 2022, 21 (3), 181–200. [PubMed: 35042991]

(4). Lai AC; Crews CM Induced protein degradation: an emerging drug discovery paradigm. Nat. Rev. Drug Discovery 2017, 16 (2), 101–114. [PubMed: 27885283]

(5). Liu J; Yu X; Chen H; Kaniskan H; Xie L; Chen X; Jin J; Wei W TF-DUBTACs stabilize tumor suppressor transcription factors. J. Am. Chem. Soc 2022, 144 (28), 12934–12941. [PubMed: 35786952]

(6). Henning NJ; Boike L; Spradlin JN; Ward CC; Liu G; Zhang E; Belcher BP; Brittain SM; Hesse MJ; Dovala D; McGregor LM; Valdez Misiolek R; Plasschaert LW; Rowlands DJ; Wang F; Frank AO; Fuller D; Estes AR; Randal KL; Panidapu A; McKenna JM; Tallarico JA; Schirle M; Nomura DK Deubiquitinase-targeting chimeras for targeted protein stabilization. Nat. Chem. Biol 2022, 18 (4), 412–421. [PubMed: 35210618]

(7). Siriwardena SU; Munkanatta Godage DNP; Shoba VM; Lai S; Shi M; Wu P; Chaudhary SK; Schreiber SL; Choudhary A Phosphorylation-inducing chimeric small molecules. J. Am. Chem. Soc 2020, 142 (33), 14052–14057. [PubMed: 32787262]

(8). Yamazoe S; Tom J; Fu Y; Wu W; Zeng L; Sun C; Liu Q; Lin J; Lin K; Fairbrother WJ; Staben ST Heterobifunctional molecules induce dephosphorylation of Kinases-A proof of concept study. J. Med. Chem 2020, 63 (6), 2807–2813. [PubMed: 31874036]

(9). Wang WW; Chen LY; Wozniak JM; Jadhav AM; Anderson H; Malone TE; Parker CG Targeted protein acetylation in cells using heterobifunctional molecules. J. Am. Chem. Soc 2021, 143 (40), 16700–16708. [PubMed: 34592107]

(10). Narita T; Weinert BT; Choudhary C Functions and mechanisms of non-histone protein acetylation. Nat. Rev. Mol. Cell Biol 2019, 20 (3), 156–174. [PubMed: 30467427]

(11). Chen L; Liu S; Tao Y Regulating tumor suppressor genes: post-translational modifications. Signal. Transduct. Target. Ther 2020, 5 (1), 90. [PubMed: 32532965]

(12). Markham D; Munro S; Soloway J; O'Connor DP; La Thangue NB DNA-damage-responsive acetylation of pRb regulates binding to E2F-1. EMBO Rep. 2006, 7 (2), 192–198. [PubMed: 16374512]

(13). Ikenoue T; Inoki K; Zhao B; Guan KL PTEN acetylation modulates its interaction with PDZ domain. Cancer Res. 2008, 68 (17), 6908–6912. [PubMed: 18757404]

(14). Liu Y; Gu W p53 in ferroptosis regulation: the new weapon for the old guardian. Cell Death Differ. 2022, 29 (5), 895–910. [PubMed: 35087226]

(15). Luo J; Li M; Tang Y; Laszkowska M; Roeder RG; Gu W Acetylation of p53 augments its site-specific DNA binding both in vitro and in vivo. Proc. Natl. Acad. Sci. U S A 2004, 101 (8), 2259–2264. [PubMed: 14982997]

(16). Tang Y; Zhao W; Chen Y; Zhao Y; Gu W Acetylation is indispensable for p53 activation. Cell 2008, 133 (4), 612–626. [PubMed: 18485870]

(17). Wang SJ; Li D; Ou Y; Jiang L; Chen Y; Zhao Y; Gu W Acetylation Is Crucial for p53-Mediated Ferroptosis and Tumor Suppression. Cell Rep. 2016, 17 (2), 366–373. [PubMed: 27705786]

(18). Nabet B; Roberts JM; Buckley DL; Paulk J; Dastjerdi S; Yang A; Leggett AL; Erb MA; Lawlor MA; Souza A; Scott TG; Vittori S; Perry JA; Qi J; Winter GE; Wong KK; Gray NS; Bradner JE The dTAG system for immediate and target-specific protein degradation. Nat. Chem. Biol 2018, 14 (5), 431–441. [PubMed: 29581585]

(19). Yang W; Rozamus LW; Narula S; Rollins CT; Yuan R; Andrade LJ; Ram MK; Phillips TB; van Schravendijk MR; Dalgarno D; Clackson T; Holt DA Investigating protein-ligand interactions with a mutant FKBP possessing a designed specificity pocket. J. Med. Chem 2000, 43 (6), 1135–1142. [PubMed: 10737745]

(20). Bullock AN; Henckel J; Fersht AR Quantitative analysis of residual folding and DNA binding in mutant p53 core domain: definition of mutant states for rescue in cancer therapy. Oncogene 2000, 19 (10), 1245–1256. [PubMed: 10713666]

(21). Boeckler FM; Joerger AC; Jaggi G; Rutherford TJ; Veprintsev DB; Fersht AR Targeted rescue of a destabilized mutant of p53 by an in silico screened drug. Proc. Natl. Acad. Sci. U S A 2008, 105 (30), 10360–10365. [PubMed: 18650397]

(22). Wilcken R; Liu X; Zimmermann MO; Rutherford TJ; Fersht AR; Joerger AC; Boeckler FM Halogen-enriched fragment libraries as leads for drug rescue of mutant p53. J. Am. Chem. Soc 2012, 134 (15), 6810–6818. [PubMed: 22439615]

(23). Liu X; Wilcken R; Joerger AC; Chuckowree IS; Amin J; Spencer J; Fersht AR Small molecule induced reactivation of mutant p53 in cancer cells. Nucleic Acids Res. 2013, 41 (12), 6034–6044. [PubMed: 23630318]

(24). Baud MGJ; Bauer MR; Verduci L; Dingler FA; Patel KJ; Horil Roy D; Joerger AC; Fersht AR Aminobenzothiazole derivatives stabilize the thermolabile p53 cancer mutant Y220C and show anticancer activity in p53-Y220C cell lines. Eur. J. Med. Chem 2018, 152, 101–114. [PubMed: 29702446]

(25). Bauer MR; Krämer A; Settanni G; Jones RN; Ni X; Khan Tareque R; Fersht AR; Spencer J; Joerger AC Targeting cavity-creating p53 cancer mutations with small-molecule stabilizers: the Y220X paradigm. ACS Chem. Biol 2020, 15 (3), 657–668. [PubMed: 31990523]

(26). Bauer MR; Jones RN; Tareque RK; Springett B; Dingler FA; Verduci L; Patel KJ; Fersht AR; Joerger AC; Spencer J A structure-guided molecular chaperone approach for restoring the

transcriptional activity of the p53 cancer mutant Y220C. Future Med. Chem 2019, 11 (19), 2491–2504. [PubMed: 31633398]

(27). Guiley KZ; Shokat KM A small molecule reacts with the p53 somatic mutant Y220C to rescue wild-type thermal stability. Cancer Discovery 2023, 13 (1), 56–69. [PubMed: 36197521]

(28). Basse N; Kaar JL; Settanni G; Joerger AC; Rutherford TJ; Fersht AR Toward the rational design of p53-stabilizing drugs: probing the surface of the oncogenic Y220C mutant. Chem. Biol 2010, 17 (1), 46–56. [PubMed: 20142040]

(29). Bedford DC; Kasper LH; Fukuyama T; Brindle PK Target gene context influences the transcriptional requirement for the KAT3 family of CBP and p300 histone acetyltransferases. Epigenetics 2010, 5 (1), 9–15. [PubMed: 20110770]

(30). Weinert BT; Narita T; Satpathy S; Srinivasan B; Hansen BK; Schölz C; Hamilton WB; Zucconi BE; Wang WW; Liu WR; Brickman JM; Kesicki EA; Lai A; Bromberg KD; Cole PA; Choudhary C Time-resolved analysis reveals rapid dynamics and broad scope of the CBP/p300 acetylome. Cell 2018, 174 (1), 231–244.e12. [PubMed: 29804834]

(31). Dancy BM; Cole PA Protein lysine acetylation by p300/CBP. Chem. Rev 2015, 115 (6), 2419–2452. [PubMed: 25594381]

(32). Lasko LM; Jakob CG; Edalji RP; Qiu W; Montgomery D; Digiammarino EL; Hansen TM; Risi RM; Frey R; Manaves V; Shaw B; Algire M; Hessler P; Lam LT; Uziel T; Faivre E; Ferguson D; Buchanan FG; Martin RL; Torrent M; Chiang GG; Karukurichi K; Langston JW; Weinert BT; Choudhary C; de Vries P; Kluge AF; Patane MA; Van Drie JH; Wang C; McElligott D; Kesicki E; Marmorstein R; Sun C; Cole PA; Rosenberg SH; Michaelides MR; Lai A; Bromberg KD Discovery of a selective catalytic p300/CBP inhibitor that targets lineage-specific tumours. Nature 2017, 550 (7674), 128–132. [PubMed: 28953875]

(33). Yang Y; Zhang R; Li Z; Mei L; Wan S; Ding H; Chen Z; Xing J; Feng H; Han J; Jiang H; Zheng M; Luo C; Zhou B Discovery of highly potent, selective, and orally efficacious p300/CBP histone acetyltransferases inhibitors. J. Med. Chem 2020, 63 (3), 1337–1360. [PubMed: 31910017]

(34). Crawford TD; Romero FA; Lai KW; Tsui V; Taylor AM; de Leon Boenig G; Noland CL; Murray J; Ly J; Choo EF; Hunsaker TL; Chan EW; Merchant M; Kharbanda S; Gascoigne KE; Kaufman S; Beresini MH; Liao J; Liu W; Chen KX; Chen Z; Conery AR; Côté A; Jayaram H; Jiang Y; Kiefer JR; Kleinheinz T; Li Y; Maher J; Pardo E; Poy F; Spillane KL; Wang F; Wang J; Wei X; Xu Z; Xu Z; Yen I; Zawadzke L; Zhu X; Bellon S; Cummings R; Cochran AG; Albrecht BK; Magnuson S Discovery of a potent and selective in vivo probe (GNE-272) for the bromodomains of CBP/EP300. J. Med. Chem 2016, 59 (23), 10549–10563. [PubMed: 27682507]

(35). Hay DA; Fedorov O; Martin S; Singleton DC; Tallant B; Wells C; Picaud S; Philpott M; Monteiro OP; Rogers CM; Conway SJ; Rooney TP; Tumber A; Yapp C; Filippakopoulos P; Bunnage ME; Müller S; Knapp S; Schofield CJ; Brennan PD Discovery and optimization of small-molecule ligands for the CBP/p300 bromodomains. J. Am. Chem. Soc 2014, 136 (26), 9308–9319. [PubMed: 24946055]

(36). Chiarella AM; Butler KV; Gryder BE; Lu D; Wang TA; Yu X; Pomella S; Khan J; Jin J; Hathaway NA Dose-dependent activation of gene expression is achieved using CRISPR and small molecules that recruit endogenous chromatin machinery. Nat. Biotechnol 2020, 38 (1), 50–55. [PubMed: 31712774]

(37). Ryu HW; Shin DH; Lee DH; Choi J; Han G; Lee KY; Kwon SH HDAC6 deacetylates p53 at lysines 381/382 and differentially coordinates p53-induced apoptosis. Cancer Lett. 2017, 391, 162–171. [PubMed: 28153791]

(38). Hoffmann G; Breitenbücher F; Schuler M; Ehrenhofer-Murray AE A novel sirtuin 2 (SIRT2) inhibitor with p53-dependent pro-apoptotic activity in non-small cell lung cancer. J. Biol. Chem 2014, 289 (8), 5208–16. [PubMed: 24379401]

(39). Fischer M Census and evaluation of p53 target genes. Oncogene 2017, 36 (28), 3943–3956. [PubMed: 28288132]

(40). Zhu S; Zhang Q; Sun X; Zeh HJ 3rd; Lotze MT; Kang R; Tang D HSPA5 regulates ferroptotic cell death in cancer cells. Cancer Res. 2017, 77 (8), 2064–2077. [PubMed: 28130223]

(41). Wang XW; Zhan Q; Coursen JD; Khan MA; Kontny HU; Yu L; Hollander MC; O'Connor PM; Fornace AJ Jr.; Harris CC GADD45 induction of a G2/M cell cycle checkpoint. Proc. Natl. Acad. Sci. U S A 1999, 96 (7), 3706–3711. [PubMed: 10097101]

(42). Engeland K Cell cycle regulation: p53-p21-RB signaling. Cell Death Differ. 2022, 29 (5), 946–960. [PubMed: 35361964]

(43). Kuribayashi K; Krigsfeld G; Wang W; Xu J; Mayes PA; Dicker DT; Wu GS; El-Deiry WS TNFSF10 (TRAIL), a p53 target gene that mediates p53-dependent cell death. Cancer Biol. Ther 2008, 7 (12), 2034–2038. [PubMed: 19106633]

(44). Kong LR; Ong RW; Tan TZ; Mohamed Salleh NAB; Thangavelu M; Chan JV; Koh LYJ; Periyasamy G; Lau JA; Le TBU; Wang L; Lee M; Kannan S; Verma CS; Lim CM; Chng WJ; Lane DP; Venkitaraman A; Hung HT; Cheok CD; Goh BC Targeting codon 158 p53-mutant cancers via the induction of p53 acetylation. Nat. Commun 2020, 11 (1), 2086. [PubMed: 32350249]

(45). Kwon MY; Park E; Lee SJ; Chung SW Heme oxygenase-1 accelerates erastin-induced ferroptotic cell death. Oncotarget 2015, 6 (27), 24393–24403. [PubMed: 26405158]

(46). Liu J; Song X; Kuang F; Zhang Q; Xie Y; Kang R; Kroemer G; Tang D NUPR1 is a critical repressor of ferroptosis. Nat. Commun 2021, 12 (1), 647. [PubMed: 33510144]

(47). Xiong Y; Zhong Y; Yim H; Yang X; Park KS; Xie L; Poulikakos PI; Han X; Xiong Y; Chen X; Liu J; Jin J Bridged proteolysis targeting chimera (PROTAC) enables degradation of undruggable targets. J. Am. Chem. Soc 2022, 144 (49), 22622–22632. [PubMed: 36448571]

(48). Wei J; Meng F; Park KS; Yim H; Velez J; Kumar P; Wang L; Xie L; Chen H; Shen Y; Teichman E; Li D; Wang GD ; Chen X; Kaniskan H; Jin J Harnessing the E3 ligase KEAP1 for targeted protein degradation. J. Am. Chem. Soc 2021, 143 (37), 15073–15083. [PubMed: 34520194]

(49). Park KS; Qin L; Kabir M; Luo K; Dale B; Zhong Y; Kim A; Wang GG; Kaniskan H; Jin J Targeted degradation of PRC1 components, BMI1 and RING1B, via a novel protein complex degrader strategy. Adv. Sci 2023, 10 (10), No. e2205573.

(50). Ma A; Stratikopoulos E; Park KS; Wei J; Martin TC; Yang X; Schwarz M; Leshchenko V; Rialdi A; Dale B; Lagana A; Guccione E; Parekh S; Parsons R; Jin J Discovery of a first-in-class EZH2 selective degrader. Nat. Chem. Biol 2020, 16 (2), 214–222. [PubMed: 31819273]

(51). Patro R; Duggal G; Love MI; Irizarry RA; Kingsford C Salmon provides fast and bias-aware quantification of transcript expression. Nat. Methods 2017, 14 (4), 417–419. [PubMed: 28263959]

(52). Weinstein JN; Collisson EA; Mills GB; Shaw KR; Ozenberger BA; Ellrott K; Shmulevich I; Sander C; Stuart JM The cancer genome atlas pan-cancer analysis project. Nat. Genet 2013, 45 (10), 1113–1120. [PubMed: 24071849]

(53). Soneson C; Love MI; Robinson MD Differential analyses for RNA-seq: transcript-level estimates improve gene-level inferences. F1000Res. 2015, 4, 1521. [PubMed: 26925227]

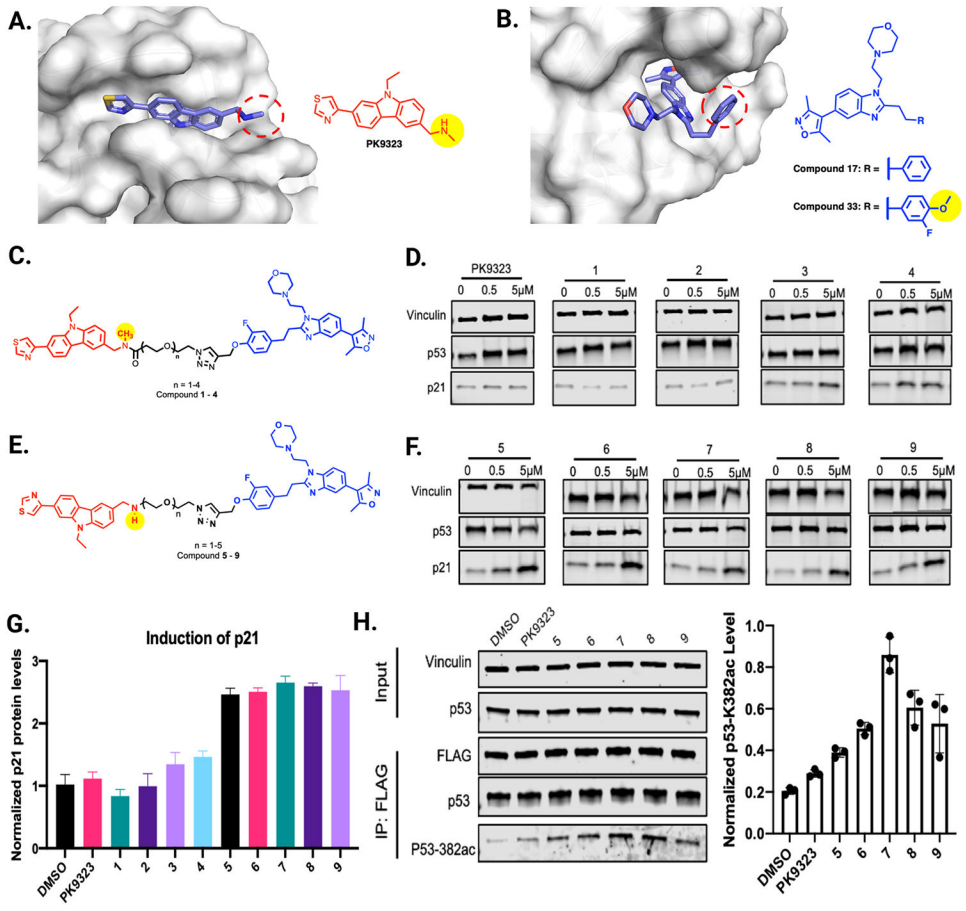

Figure 1.

Design and testing of initial p53Y220C-targeting AceTACs. (A) Crystal structure of the p53Y220C-PK9323 complex (PDB ID: 6SI0).[25] The cross-section of the occupied binding pocket is highlighted, and the structure of PK9323 is shown. (B) Crystal structure of the CBP bromodomain compound **17** complex (PDB ID: 4NR5).[35] The cross-section of the occupied binding pocket is highlighted, and the structures of compounds **17** and **33** are also shown. (C) Chemical structure of compounds **1–4**. (D) Representative Western blot (WB) results of PK9323 and compounds **1–4** on inducing p21 protein expression from three independent experiments. NCI-H1299 (p53Y220C) stable cells were treated with the indicated compounds at the indicated concentrations for 24 h. (E) Chemical structure of compounds **5–9**. (F) Representative WB results of compounds **5–9** on inducing p21 protein expression from three independent experiments. NCI-H1299 (p53Y220C) stable cells were treated with the indicated compounds at the indicated concentrations for 24 h. (G) Quantification of p21 induction (from panels D and F) by PK9323 and compounds **1–9** at the 24 h time point, following 5 μM treatment (from three independent experiments). (H) Left: representative WB results of the p53K382ac level following the treatment with the indicated compounds at 5 μM for 8 h from three independent experiments. NCI-H1299 (p53Y220C) stable cells were treated with the indicated compounds for 8 h, followed by endogenous immunoprecipitation (IP) FLAG pulldown. Right: quantification of the normalized p53K382ac level (p53K382ac level over total p53 protein level) following

treatment with the indicated compounds at 5 μM for 8 h (from three independent experiments).

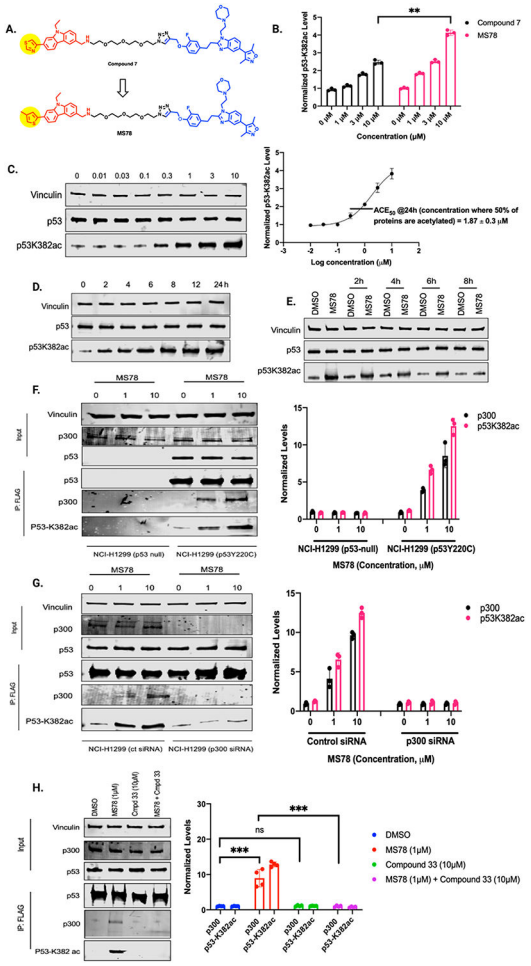

Figure 2.

Discovery and characterization of MS78, an effective p53Y220C AceTAC. (A) Chemical structure of MS78, derived from compound **7**. (B) Comparison of the normalized p53K382ac level between compound **7** and MS78 in NCI-H1299 (p53Y220C) cells treated with the indicated compounds at 0, 1, 3, or 10 μM for 24 h. Results shown are the mean values ± SD from three independent experiments (** $P < 0.01$). (C) Left: WB results of the p53K382ac level in NCI-H1299 (p53Y220C) cells treated with MS78 at the indicated concentrations at 24 h. Results shown are representative of three independent experiments. Right: quantification of the normalized p53K382ac level on the left. Results shown are the mean values ± SD from three independent experiments. (D) WB results of the p53K382ac level in NCI-H1299 (p53Y220C) cells treated with 10 μM MS78 at the indicated time points. Results shown are representative of three independent experiments. (E) WB result of the p53K382ac level at the indicated time points post treatment of NCI-H1299 (p53Y220C) cells with MS78 at 10 μM for 6 h. Results shown are representative of three independent experiments. (F) Left: WB results of MS78-mediated p53-p300 interaction via p53-FLAG pull-down in NCI-H1299 (p53-null) and NCI-H1299 (p53Y220C) cells treated with MS78 at the indicated concentrations for 24 h. Results shown are representative of three independent experiments. Right: quantification of normalized p300 and p53K382ac levels from three independent experiments shown on the left. (G) Left: WB results of

p53-FLAG pull-down after treatment of NCI-H1299 (p53Y220C) cells with MS78 at the indicated concentrations and with control siRNA or p300 siRNA. Results shown are representative of three independent experiments. Right: quantification of normalized p300 and p53K382ac levels from three independent experiments shown on the left. (H) Left: WB results of p53-FLAG pulldown after treatment of NCI-H1299 (p53Y220C) cells with MS78 alone at 1 μM, compound **33** alone at 10 μM, or compound **33** pretreatment at 10 μM for 2 h, followed by MS78 treatment at 1 μM for 18 h. Results shown are representative of four independent experiments. Right: quantification of the p300 and normalized p53K382ac levels from four independent experiments shown on the left (***$P < 0.001$).

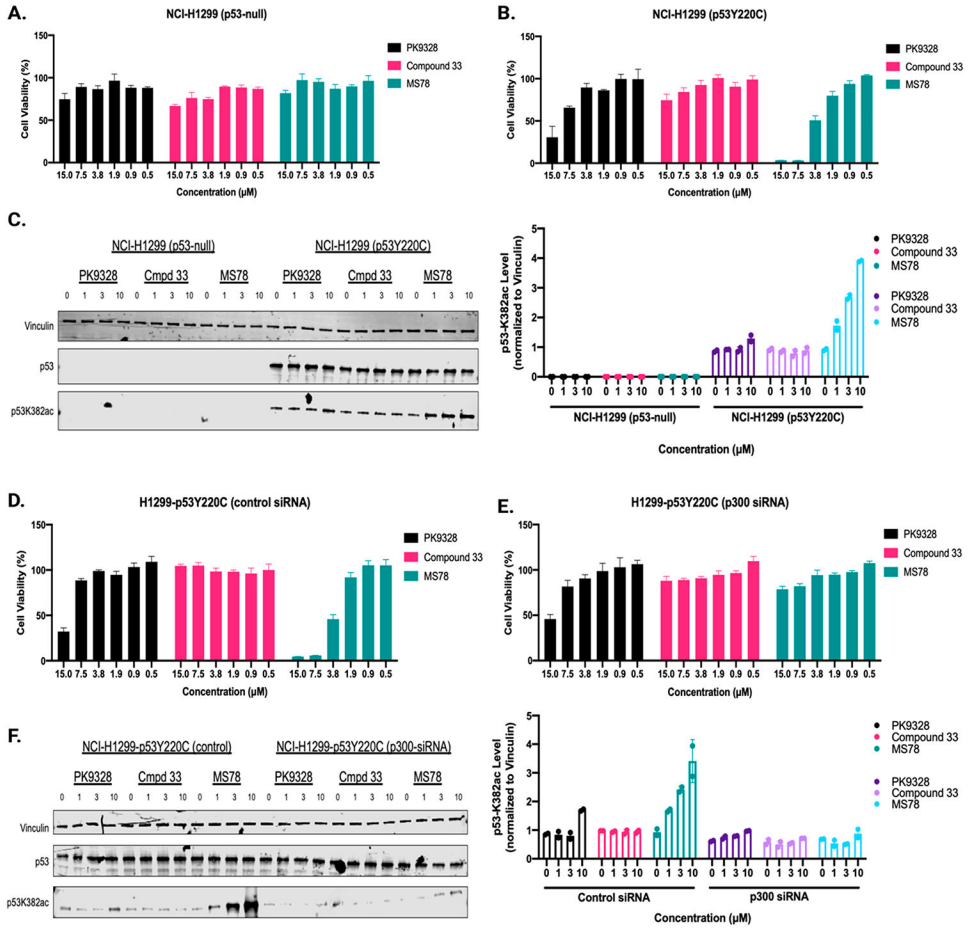

Figure 3.

MS78 inhibits cell growth in NCI-H1299 p53Y220C cells but not in NCI-H1299 p53-null cells. Cell viability of MS78, PK9328, and compound **33** in (A) NCI-H1299 p53-null and (B) NCI-H1299 p53Y220C cells. The cells were treated with the indicated compounds at the indicated concentrations for 72 h. The mean values ± SD from three independent experiments are shown. (C) Left, representative WB results of the p53K282ac level induced by MS78, PK9328, and compound **33** at 0, 1, 3, and 10 μM in NCI-H1299 p53-null and NCI-H1299 p53Y220C cells (24 treatment). Right, quantification of the p53K382ac protein level normalized to Vinculin from two independent experiments. Cell viability of MS78, PK9328, and compound **33** in NCI-H1299 p53Y220C cells treated with (D) control siRNA or (E) p300-siRNA. The cells were treated with siRNA for 72 h and then treated with the indicated compounds at the indicated concentrations for 72 h. The mean values ± SD from three independent experiments are shown. (F) Left, representative WB results of the p53K282ac level in NCI-H1299 p53Y220C cells treated with control siRNA or p300-siRNA and then treated with MS78, PK9328, or compound **33** at 0, 1, 3, and 10 μM for 24 h. Right, quantification of the p53K382ac protein level normalized to Vinculin from two independent experiments.

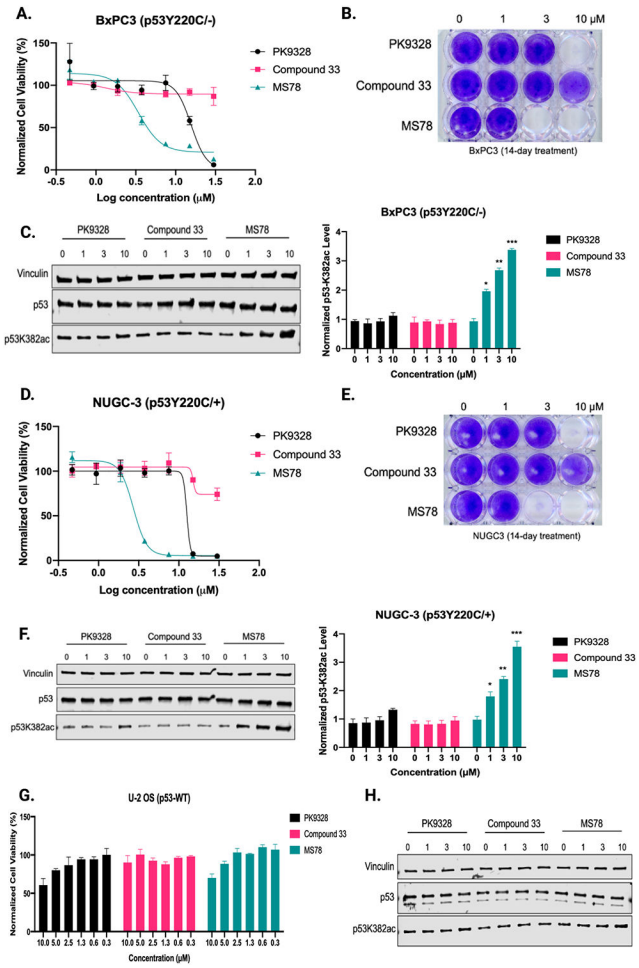

Figure 4.

MS78 effectively inhibits cell growth in cancer cell lines that endogenously express p53Y220C and is nontoxic in WT p53 cells. (A) Cell viability results of MS78, PK9328, and compound **33** in BxPC3 cells, which were treated with DMSO or the indicated compounds at the indicated concentrations for 72 h. The mean value ± SD for each concentration point (in technical triplicates from three biological experiments) is shown in the curves. GraphPad Prism 8 was used in analysis of raw data. (B) Clonogenic assay results of MS78, PK9328, and compound **33** in BxPC3 cells treated with DMSO or 1, 3, or 10 μM of the indicated compounds for 14 days. Cells were fixed and stained with crystal violet, and the images are representative of two independent experiments. (C) Left: representative WB results of the p53K382ac protein level in BxPC3 cells treated with MS78, PK9328, or compound **33** at 0, 1, 3, or 10 μM for 24 h. Right: quantification of the normalized p53K382ac level in BxPC3 cells from three independent experiments. $*P < 0.05$, $**P < 0.01$, $***P < 0.001$. (D) Cell viability results of MS78, PK9328, and compound **33** in NUGC-3 cells treated with DMSO or the indicated compounds at the indicated concentrations for 72 h. The mean value ± SD for each concentration point (in technical triplicates from three biological experiments) is shown in the curves. GraphPad Prism 8 was used in analysis of raw data. (E) Clonogenic assay results of MS78, PK9328, and compound **33** in NUGC-3 cells treated with DMSO

or 1, 3, or 10 μM of the indicated compounds for 14 days. Cells were fixed and stained with crystal violet, and the images are representative of two independent experiments. (F) Left: representative WB results of the p53K382ac protein level in NUGC-3 cells treated with MS78, PK9328, or compound **33** at 0, 1, 3, or 10 μM for 24 h. Right: quantification of the normalized p53K382ac level in NUGC-3 cells from three independent experiments. *P < 0.05, **P < 0.01, ***P < 0.001. (G) Cell viability assay results of MS78, PK9328, and compound **33** in U-2OS cells treated with the indicated compounds at the indicated concentrations for 72 h. The mean value ± SD for each concentration point (in technical triplicates from two biological experiments) is shown in the bar graph. (H) WB results of the p53K382ac protein level in U-2OS cells treated with MS78, PK9328, or compound **33** at 0, 1, 3, and 10 μM for 24 h. WB results shown are representative of two independent experiments.

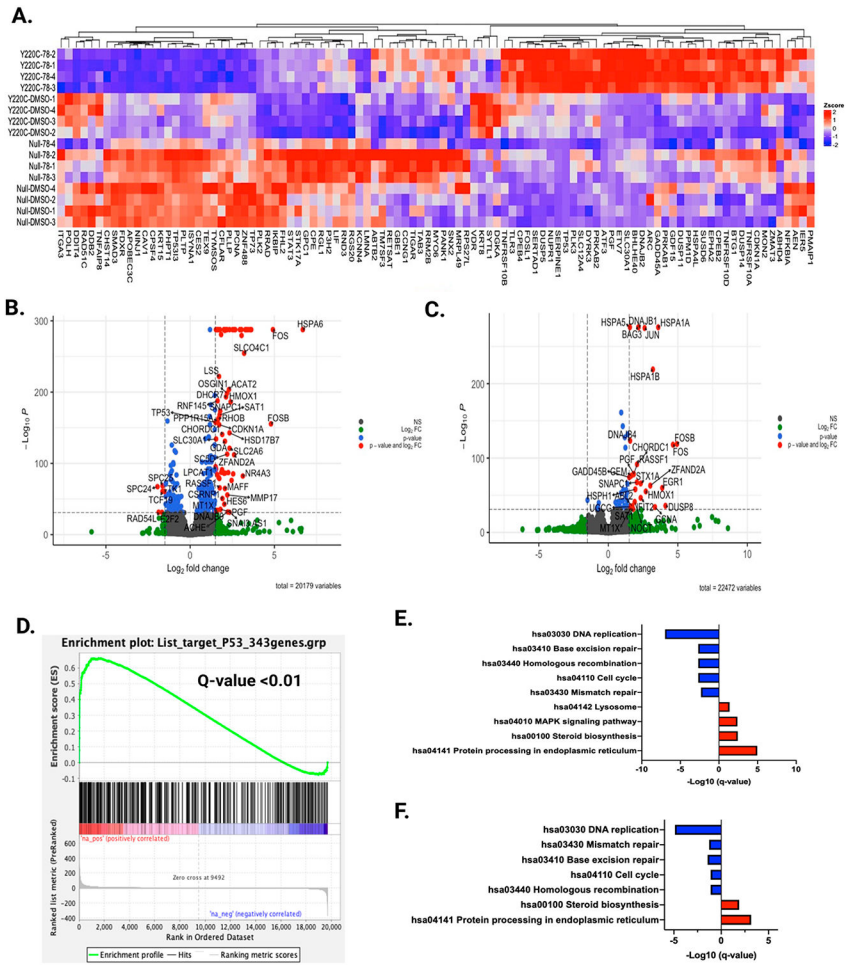

Figure 5.

The p53Y220C AceTAC MS78 induces downstream signaling of canonical and noncanonical p53 pathways. (A) Heatmap enrichment in high-confidence p53-target genes. NCI-H1299 p53-null and p53Y220C cell lines were treated with DMSO or 10 μM MS78 for 24 h in quadruplicate. (B) Volcano plot of differential gene expression (DGE) of upregulated protein and pathways upon 10 μM MS78 treatment compared to DMSO for 24 h in NCI-H1299 p53Y220C cells. (C) Volcano plot of DGE of upregulated protein and pathways upon 10 μM MS78 treatment in NCI-H1299 p53Y220C cells compared to 10 μM MS78 treatment in NCI-H1299 p53-null cells and DMSO treatment in both cell lines. (D) Enrichment plot of significant genes upregulated from the 343 high-confidence p53-target genes (q-value < 0.01, normalized enrichment score (NES) = 1.52) in NCI-H1299 p53Y220C cells treated with 10 μM MS78 versus DMSO for 24 h in quadruplicate. (E) KEGG pathway analysis of upregulated protein and pathways upon 10 μM MS78 treatment compared to DMSO for 24 h in NCI-H1299 p53Y220C cells. (F) KEGG pathway analysis of upregulated protein and pathways upon 10 μM MS78 treatment in NCI-H1299 p53Y220C stable cell line compared to DMSO treatment in NCI-H1299 p53Y220C cells, DMSO treatment in NCI-H1299 p53-null cells, and 10 μM MS78 treatment in NCI-H1299 p53-null cells. The values of $\log_2$

fold change and $\log_{10}$ *p*-values in panels B and C were generated from four independent experiments.